Journal Name

ARTICLE

Galvanic Replacement of Sub 20 nm Ag Nanoparticles in Organic Media

Received 00th January 20xx,
Accepted 00th January 20xx

DOI: 10.1039/x0xx00000x

www.rsc.org/

G. Collins, [a, b, *] E. K. McCarty[b] and J. D. Holmes [a, b]

Galvanic replacement is a versatile synthetic strategy for the synthesis of alloy and hollow nanostructures. The structural evolution of single crystalline and multiply twinned nanoparticles < 20 nm in diameter and capped with oleylamine is systematically studied. Changes in chemical composition are dependent on size and crystallinity of the parent nanoparticle. The effects of reaction temperature and rate of precursor addition are also investigated. Galvanic replacement of single crystal spherical and truncated cubic nanoparticles follow the same mechanism to form hollow octahedral nanoparticles, a mechanism which is not observed for galvanic replacement of Ag templates in aqueous systems. Multiply twinned nanoparticles can form nanorings or solid alloys by manipulating the reaction conditions. Oleylamine capped Ag nanoparticles are a highly adaptable template to synthesize a range of hollow and alloy nanostructures with tuneable localised surface plasmon resonance.

Introduction

Noble metal nanoparticles (NPs) and their alloys are of interest to wide range of areas such as electronics[1], photovoltaics[2], biomedical and catalysis[3]. Silver (Ag) and gold (Au) NPs are particularly important due to their unique optical properties which enables a range of applications such as surface enhanced Raman scattering (SERS)[4], plasmonic sensors[5], bioimaging and cancer therapy.[6] The localised surface plasmon resonance (LSPR) is highly sensitive to changes in NP shape and/or chemical composition, thereby allowing the optical properties to be tuned through alloying or manipulating their morphology. Galvanic replacement of the Ag templates is a powerful method to access a range of AgAu alloy nanostructures with unconventional morphologies such as hollow nanostructures.[7, 8] The optical properties of NPs can be dramatically red shifted, which is has been exploited for biomedical applications.[6] Hollow and porous NPs are also useful for catalytic applications due to their high surface area and potential for synergistic effects associated with alloy NPs.[9]

Galvanic replacement is driven by the difference in reduction potentials between two metals. Addition of metal cations to a solution of NPs with a higher reduction *i.e.* less noble, results in the oxidation and dissolution of the less noble metal and concurrent reduction and deposition of the more noble species. Deposition and dissolution processes are dependent on the size, shape, crystallinity and the surface chemistry of the silver NP. Due to the 1:3 ratio of Ag to Au species, for every atom of Au deposited 3 atoms of Ag are oxidised resulting in the injection of vacancies at the interface.[10] These vacancies significantly facilitate the migration of Au and Ag atoms. As the concentration of vacancies increase, they coalesce to form pinholes at the surface that serve as sites for further Ag oxidation and dissolution. Facet selective etching and growth impact on the reaction mechanism and final morphology of the NP after galvanic replacement.[8] Voids can also form via the Kirkendall effect due to differences in diffusion rates between two components in a diffusion couple.[11] Faster outward diffusion of a component than the inward diffusion of a second component, is accompanied by an inward flux of vacancies, which coalesce to form voids. A combination of galvanic replacement and Kirkendall growth can occur at different stages of the reaction and have been exploited to tune the composition and shape of NPs.[7]

Galvanic replacement of Ag NPs has been well studied in aqueous systems[12, 13] however, these reactions have been less intensively studied in organic media. The synthesis of Ag NPs in organic media is attractive due to the good monodisersity and small NP diameters achievable.[14] Furthermore, organic based synthesis typically use capping ligands such as oleylamine, which can be more easily removed compared to polymer based capping ligands, and may be useful for applications including SERS, sensing and catalysis. Within the reports of galvanic replacement in organic media a variety morphologies and compositions have been reported. Alloy nanocages and nanorings formed from 18 nm, 14 nm and 8 nm Ag NPs.[15, 16] In contrast, Yang *et al.*[17] reported 10 nm spherical Ag NPs gave core-shell NPs with only 7% of the NPs having visible voids in

[a] *Department of Chemistry and the Tyndall National Institute, University College Cork, Cork, Ireland. Email: g.collins@ucc.ie*
[b] *AMBER@CRANN, Trinity College Dublin, Dublin, Ireland.*
† Footnotes relating to the title and/or authors should appear here.
Electronic Supplementary Information (ESI) available: supplementary information available should be included here]. See DOI: 10.1039/x0xx00000x

TEM. Complete dealloying was observed for 11 nm single crystal NPs to form hollow Au octahedra.[18] Galvanic replacement of 40 nm decahedra and 50 nm triangular prisms produced hollow alloys and preserved the shape of the Ag template.[19] Hong *et al.*[20] showed that 40 nm single crystal spherical Ag NPs transformed into $Au_{30}Ag_{70}$ octahedral nanoframes in the presence of CuCl, however their procedure using 20 nm NPs did not produce hollow structures but solid octahedra. Recent studies on galvanic replacement of 24 nm cubic NPs showed the Ag template transformed to an octahedral geometry.[21] Mechanistic aspects of galvanic replacement in organic media have not been fully elucidated, and further studies into the how reaction conditions influence structural evaluation and impact on the NP chemical composition would be useful. In this work we focus on galvanic replacement reactions of Ag NPs < 20 nm in diameter. We evaluate how changes in morphology, chemical composition and optical properties are influenced as a function of size, crystallinity and reaction conditions. Different reactivity trends are observed for single crystalline and MTPs. The sensitivity of the galvanic replacement towards reaction temperature and rate of precursor addition was also investigated. Ag NPs in organic media is a versatile system that can be converted into alloy octahedral nanocages, hollow truncated octahedra, nanorings, nanocages or solid alloy NPs.

Experimental

Chemicals

Silver nitrate ($AgNO_3$), silver acetate (AcOAg) silver trifluroacetate (CF_3COOAg), gold chloride ($AuCl_3$), gold chloride hydrate ($HAuCl4.xH_2O$), and oleylamine (OAm) were purchased from Sigma Aldrich. Hexadecanediol was purchased from ABCRF. Solvents isoamylether, ortho-dichlorobenzene (DCB), ethanol, and toluene were purchased from Sigma Aldrich.

Synthetic Procedures: *Synthesis of single crystalline Ag NPs:* Single crystal Ag NPs were prepared in presence of air and $FeCl_3$ as an etchant, as previously described.[22] Briefly, 0.1 mmol $AgCO_2CF_3$, 1 ml OAm and 5 ml of isoamylether were placed in a flask and heated to 100 °C for 20 min, afterwhich time 5 umol of $FeCl_3$ in 0.5 ml isoamylether was rapidly injected. The solution was transferred into a heating mantel pre-heated to 160 °C and aged for 60 min. After the reaction cooled to room temperature, the NPs were precipitated by the addition of methanol and collected by centrifuge for 20 min at 10000 rpm. The NPs were washed twice with ethanol and collected by centrifuge for 15 min at 9000 rpm. The NPs were re-dispersed in toluene. Synthesis of 9 nm Ag NPs was carried out using a modified literature method.[18] A solution containing 1 ml of OAm, 10 ml o-DCB and 300 mg of 1,2 hexadecanediol was heated to 160 °C. Solution of 0.2 mmol $AgCO_2CF_3$ in 1 ml OAm in 5 ml of DCB and 5 *u*mol $FeCl_3$ in 0.5 ml in DCB were co-injected into the diol solution under rapid stirring. The reaction was aged for 30 min and the NPs collected as previously described.

Synthesis of multiply twinned Ag NPs: For the synthesis of all MTPs, Ar was bubbled through the reaction mixture for the duration of the reaction. 15 nm MTP were prepared by a method previously described.[22] Briefly, 0.1 mmol of $AgCO_2CF_3$, 0.66 ml of OAm and 10 ml isoamyl ether were heated under a gentle Ar stream, to 50 °C. The solution was then heated to 160 °C at a rate of 3-5 C min^{-1}. 8 nm MTP was prepared as previous described[21] by mixing 0.2 mmol of $AgNO_3$, 2 mmol of OAm and 15 ml of *o*-DCB. The solution was then heated at a rate of 3-5 °C min^{-1} to 160 °C and aged for 1 h. After cooling to room temperature the NPs were collected and purified as previously described. 6 nm MTP were prepared by the heating 0.1 mmol of $AgCO_2CF_3$, 2 ml of OAm in isoamylether to 140 °C for 30 min. After the reaction ethanol was added and the solution was centrifuged at 2000 rpm for 5 min to precipitate the larger NPs. Size selective precipitation of the supernatant as described by Peng[23] was carried out to narrow the NP size distribution.

Galvanic replacement: A fresh 0.2 mM solution of $AuCl_3$ was prepared by dissolving 3.4 mg of $AuCl_3$ and 2 ml of OAm in 48 ml of DCB. Nanoparticle stock solutions of 1 mg ml^{-1} were prepared in toluene. 200 µl of Ag NPs solution was added to 4 ml of toluene, followed by 100 ul of OAm heated to 60 °C under magnetic stirring. Different volumes of Au solution (0.1 ml, 0.25 ml, 0.5 ml, 1 ml, 1.5 ml) were added dropwise using an auto injector at a rate of 0.1 ml min^{-1} or manually. After the addition of the precursor, the solutions were left to age at 60 °C for 15 min. The NPs were left to cool to room temperature and precipitated by addition of ethanol and collected by centrifuge at 9000 rpm for 5 min. The NPs were washed twice with ethanol and re-dispersed in toluene.

Materials Characterisation

Transmission electron microscopy (TEM) analysis was performed using a Jeol 2100 electron microscope at an operating voltage of 200 kV. Elemental mapping was performed using energy dispersive X-ray spectroscopy (EDX). NPs were characterised by UV-visible spectroscopy using a Thermo Scientific Evolution 60S UV-Visible spectrophotometer.

Results and discussion

Ag Nanoparticle Synthesis

Controlled synthesis of Ag NPs in organic media has been extensively studied and will not be considered here in detail.[14] MTPs with an icosahedral shape, characterised by 20 surface facets are thermodynamically favoured at small diameters. The synthesis of single crystalline NPs in organic media can be achieved by the addition of etchants which include O_2, by carrying out the reaction in air or by the presence of additives such as Fe^{3+} and Cl^- ions.[22] These ions promote the oxidative etching of twinned nuclei due to the higher reactivity of these defects towards, producing defect-free surfaces of the single crystal nuclei that continue to grow into spherical NPs that have a truncated cuboctahedral shape.[14] In this study, 16 nm single crystal NPs co-existed with about 10% of multiply twinned particles due to competing reaction pathways. It is interesting to note that for the 9 nm single crystalline NPs prepared in o-DCB solvent, the use of p-DCB was not an effective solvent. It has been suggested that dissociation of C-Cl bond results in Cl- ions which act as oxidative etchants.[21] Furthermore, $AgNO_3$ was found to be superior to $AgCO_2CF_3$ or AgOAc in producing single crystal NPs, possibly due to the additional etching power of NO_3^- species. However, addition of $FeCl_3$ to these precursors did lead to single crystal NPs. Rapid injection lead to formation of single crystal nanoparticles with few multiply twinned particles were observed.[18]

Galvanic Replacement of Single Crystal Ag Nanoparticles

Fig. 1a shows a TEM image of single crystal Ag NPs with a mean diameter of 16.4 nm (standard deviation, σ=1.6 nm). Dropwise addition of 0.2 mM $AuCl_3$ solution in DCB resulted in the appearance of random voids and the formation of a shell with darker contrast is clearly observed in the TEM image in Fig. 1b, after the addition of 0.25 ml of Au precursor. A transition from the spherical shaped template to a faceted morphology can also be observed on some NPs. As the reaction continues with the addition of further Au precursor, the voids grew and coalesced and the {111} facets increased in size forming well-defined octahedra, as shown in the TEM image in Fig. 1c. The hollow NPs are single crystalline, confirmed by the Fourier transform pattern (Fig. 1 d). Most of the hollow NPs are orientated along the [110] zone axis on the TEM grid, making the octahedral geometry readily identifiable. The average length across the octahedra (determined for particles projected along [110] direction, is 27 nm (σ=2.2 nm) which is significantly greater than the original Ag template. Preferential growth occurs on the {100} facets, which is consistent with the surface energies of the low-index facets $\gamma\{111\} < \gamma\{100\} < \gamma\{110\}$. Elemental mapping by EDX, shown in Fig. 1e confirms that the octahedral nanocages are AgAu alloy with a composition of $Ag_{30}Au_{70}$. Morphological and chemical composition changes due to galvanic replacement resulted in the characteristic red shift of the LSPR, as shown in Fig. 1g. The hollow octahedra, which are blue-green in colour have a maximum absorption at 706 nm.

Recently, cubic NPs with a length of 24 nm were reported to form hollow octahedra on galvanic replacement, suggesting a similar mechanism to the spherical NPs. To investigate how the morphology of the template impacts on the final NP morphology,

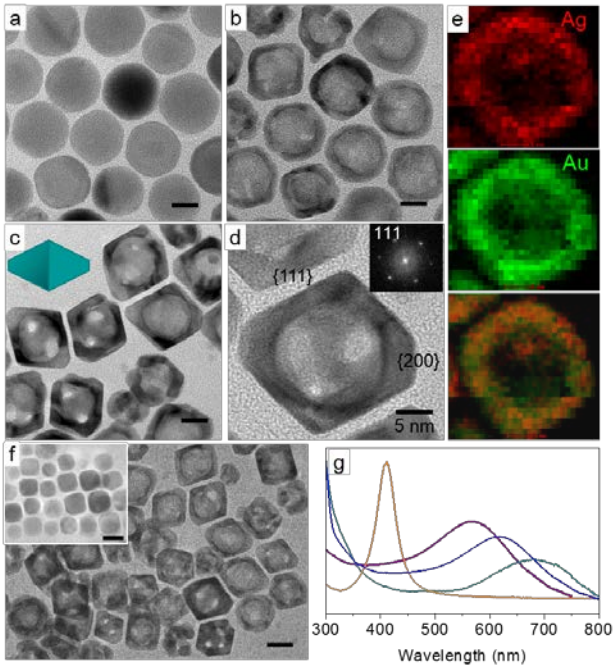

Fig. 1 TEM image of (a) single crystal Ag NPs. After dropwise addition of (b) 0.25 ml and (c) 1 ml of $AuCl_3$. Scale bar a-c is 10 nm. (d) HRTEM of hollow octahedral NP. (e) Elemental EDX mapping of octahedral NPs. (f) galvanic replacement of truncated cubic NPs. Inset: truncated cubic NPs. Scale bar is 10 nm. (g) UV-vis spectra of NPs showing red-shift in LSPR.

cubic NPs of similar size to the spherical NPs were prepared. Sub-20 nm truncated cubic NPs can be formed by decreasing the amount of $FeCl_3$ etchant added during the reaction,[22] resulting in cubic NPs with an average length of 14 nm, shown in Fig. 1f inset. This synthesis produces ~15% contribution of single crystal spherical and MTP NPs but allows for comparable NP size. Galvanic displacement of the truncated cubic NPs produce the same hollow octahedra, as shown in Fig. 3b. These observations, indicate that a hollow octahedral morphology is favoured regardless of whether the initial Ag NP is spherical or cubic. This mechanism is very different from that of the well-studied PVP-capped Ag NPs in aqueous solutions where cubic NPs form hollow boxes,[12] where the reaction is initiated on the {111} surface facets of truncated cubes. Recent 3D EDX mapping of cubic NPs revealed pinhole formation can indeed be initiated on {100} facets.[24] The presence of surface openings can be seen on the {200} facets in Fig. 1b. These pinholes disappear as the reaction continues due to the diffusion and deposition of Au onto the {100} facets, resulting in an epitaxial shell.

The influence of reaction conditions was investigated by changing the rate of precursor addition and reaction temperature. Addition of the Au precursor was varied using a single addition rather than a dropwise addition. The rate of precursor addition is important as higher concentrations of Au^{3+} increase the reaction rate of galvanic replacement, thereby affecting the rates of

dissolution and deposition which impact on the final NP morphology. The rate of reaction can be critical for achieving selective deposition.[25] Fig S1 shows Ag NPs after rapid addition of 1 ml $AuCl_3$ did not sufficiently impact on the morphology. Evidence of homogeneous nucleation of Au was indicated by the presence of small diameter NPs but hollow octahedra were still observed (Fig. S1a and 1b), although the facets were more rounded. The relative insensitivity to Au injection rate may be due to OAm acting as a complexing agent with the Au, slowing the reduction rate of Au and allowing for kinetically controlled growth. CTAB has been shown to retard the rate of Au reduction in aqueous replacement reactions through complexation.[26] An evaluated reaction temperature was required for the reaction. Galvanic replacement reactions conducted at room temperature did not produce well-defined hollow structures but rough aggregated nanostructures which can be attributed to slower atomic diffusion at lower temperatures (Fig. S1c).

Size effects in galvanic replacement of single crystal NPs were studied by conducting the same procedure on 8.8 nm NP (σ=2.1), as shown in the TEM image Fig. 2a inset. Fig. 2a shows a TEM image of NPs after addition of 1.5 ml of Au. Galvanic replacement gives mixed hollow truncated octahedral and cuboctahedral nanocrystals. The NPs assume random orientations on the TEM grid making their morphology less readily identifiable, compared to the larger Ag templates. HRTEM images shown in Fig. 2d and 2e, show a hollow truncated octahedral and cuboctahedral NP viewed along the [110] direction, respectively. The average alloy composition determined by EDX was $Ag_{15}Au_{85}$. Chemical compositional profiles across the NPs, shown in Fig. 2c indicate an alloy of uniform composition. The average length of the octahedral NPs measured 12.7 nm, again indicating net growth along the [200] direction. While the larger single crystal NPs exclusively form hollow octahedral nanocages, with voids on the {111} surface facets, many of the smaller NPs form octahedral nanorings as the voids coalesce to form a single void, which can be seen in Fig. 2b. Shape evolution towards an octahedral morphology is apparent but the majority of particles are heavily truncated. The 8 nm NPs are capped with mixed OAm and hexadecanediol (HDD), while the 16 nm NPs are capped with OAm, therefore it was investigated if differences in the growth originate from the surface capping ligands which can impact on the growth and etching of surface facets and also influence galvanic replacement.[15] Ligand exchange of HDD with OAm was carried out by sonicating in a toluene solution of OAm. Subsequent galvanic replacement reaction yielded similar hollow nanostructures (Fig. S2) indicating negligible impact of these two capping ligands. In addition to the degree of truncation, another structural difference is the size of the central void in the octahedral NPs. The larger Ag templates have voids ~14 nm in diameter, similar to that of the original NP. Considerably smaller void interiors, ~1-4 nm, are observed for the 9 nm NPs. It should be noted that the void sizes can only been taken as an estimate based on the 2 dimensional representation of the NPs obtained in TEM. In either case, this observation indicates greater inward diffusion of Au for smaller NPs. The chemical compositional

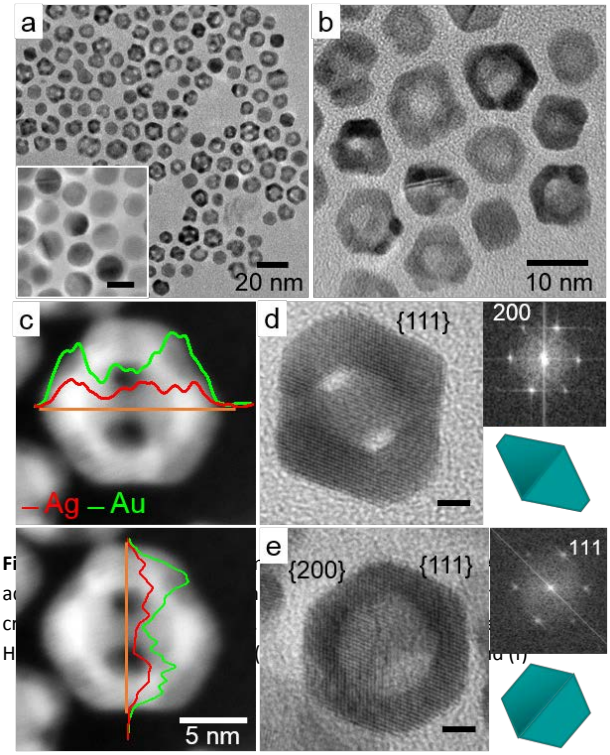

changes associated with the galvanic replacement are also size dependent, with a greater Au content achievable on smaller NP diameters, under the same reaction conditions. Equation 1 gives the size dependent Boltzmann-Arrhenius dependence of diffusivity (D_0) on temperature (T)[27]

where ΔH_D is the activation enthalpy, k_B is the Boltzmann constant, D_0 is the pre-exponential factor, r and R are the diameter of the atom and NP, respectively. Equation 1 implies that diffusion will increase with increasing temperature and diffusivity will be larger for smaller diameter NPs, consistent with the observed reactivity trend.

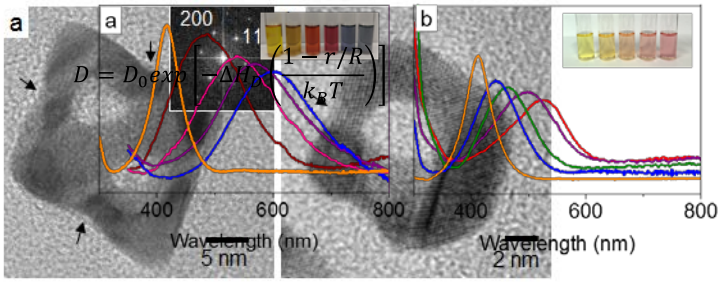

Fig. 5 UV-vis spectra of (a) 14 nm MTP and (b) 6 nm MTPs after

Fig. 3. Pinhole formation on {111} facet of (a) octahedral nanocage and hotograph of (b) octahedral nanoring.

Continued addition of Au precursor lead to fragmentation of the hollow NPs due to dealloying and solution changed from green-blue to pink. In the later stages of the reaction dealloying forms pinholes on the {111} facets, which has been observed in many systems[8] and can be readily identified in TEM images shown in Fig. 3a and 3b for 16 nm and 9 nm NPs, respectively. Pinhole formation arises from Kirkendall growth due to the faster outward diffusion of Ag than inward diffusion of Au.

Galvanic Replacement of Multiply Twinned Ag Nanoparticles

Galvanic replacement of MTPs was evaluated using 14.8 (σ= 1.3) nm, 8.4 nm (σ= 0.9) and 6.1 nm (σ= 0.8) MTPs, as shown in Fig. 4a, 4d and 4g, respectively. Galvanic replacement gives hollow NPs for 15 nm and 8 nm, while 6 nm NPs form solid alloy spherical NPs. Xia and co-workers[15] have previously studied size effects for 14 nm and 8 nm MTPs reporting that the reaction is initiated on the {111} surface facets and nanocages arise from decahedral parent NPs while nanocages formed from icosahedral shaped parent NPs. Similar structures are observed in Fig. 4b

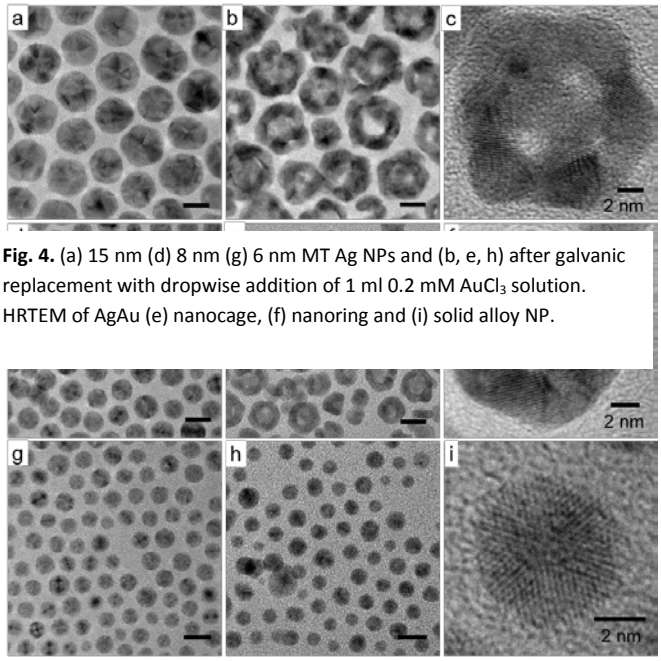

Fig. 4. (a) 15 nm (d) 8 nm (g) 6 nm MT Ag NPs and (b, e, h) after galvanic replacement with dropwise addition of 1 ml 0.2 mM $AuCl_3$ solution. HRTEM of AgAu (e) nanocage, (f) nanoring and (i) solid alloy NP.

and 4c with nanocages more prevalent for larger NPs due to greater stability of the larger template as. Nanorings characterised by smooth surfaces are more prevalent for smaller diameter templates are as shown in Fig. 4e and 4f. The morphological changes could also be conveniently tracked by monitoring the LSPR, as shown in the UV-vis spectra, in Fig. 5a. Hollow NPs change from yellow, to orange, purple and finally blue, with further addition giving a red-pink colour solution due to fragmentation. Chemical compositional changes for hollow NPs are dependent on the crystallinity of the template. The Au composition obtainable for MTPs is lower than that of the single crystalline NPs. EDX analysis of the NPs show the average composition to be $Ag_{66}Au_{33}$. EDX area maps and line scans taken across several NPs, such as those shown in Fig. S6a indicate the Au and Ag ratio is not uniform throughout the NP, which can be attributed to their polycrystalline structure.

Galvanic displacement of 6 nm NPs under the same conditions produced solid alloy NPs, as shown in the TEM image in Fig. 4h. The NPs retained the monodispersity of the parent NP and HRTEM, shown in Fig. 6i confirms the NPs are icosahedral in shape, retaining the morphology of the Ag template also. The average size of the NPs decreased to 5.8 nm after addition of 0.5 ml and 5.2 nm after addition of 1.5 ml of Au precursor. Formation of solid alloy NPs progressively shifts the LSPR to 520 nm with increasing Au concentration as shown in the UV-vis spectra in Fig. 5b. A single absorption peak at a wavelength between that of Ag (~400 nm) and Au (~ 520 nm) is characteristic of alloy formation rather than a mixture of monometallic Au and Ag nanoparticles or core-shell structures, which gives two absorbance peaks.[28]

The influence of reaction conditions on the galvanic replacement of MTPs was studied. In contrast to the single crystal NPs, the rate of Au precursor addition had a significant impact on MTPs. For the 15 and 8 nm NPs rapid precursor addition and higher reaction temperature favoured solid alloy NP formation. Fig. 6b shows a TEM image of 8 nm MTPs after rapid addition of 1 ml $AuCl_3$ at 100 °C resulted in alloy NPs with a mean diameter of 7.1 nm (σ= 1.6 nm). The same procedure was less effect for the 15 nm MTPs, which produced a combination of hollow and solid NPs (Fig. S4). Similar to galvanic replacement of single crystal NPs, an elevated reaction temperature was necessary. Fig. S5 shows the MTPs after galvanic replacement at room temperature. While some hollow formation is observed, likely due to the vacancy-rich grain boundaries which facilitate fast diffusion even at room temperature, the NPs are mainly solid and polydisperse. In aqueous systems, elevated temperatures are required not only to promote atomic diffusion but also to solubilise the AgCl reaction by-product which can otherwise deposit on the NP surface.[13]

It is interesting to note the different reactivity trend again observed for the 6 nm MTPs. These NPs were insensitive to the rate of Au addition giving alloy NPs. Rapid addition of >80 mol% of Au precursor follows a different reaction mechanism whereby the solution turns colourless followed by the appearance of a pink colour with a single absorption at 525 nm, as shown in the UV spectrum (Fig. 6d). TEM analysis of the resulting NPs, shown in Fig 6c reveal they are quasi-spherical irregularly faceted NPs, with a mean diameter of 15.6 nm and 20% polydispersity. HRTEM, shown in Fig. 6d inset confirms the NPs are polycrystalline. EDX analysis displayed in Fig. 6e shows the NPs are Au rich alloys with a composition of $Au_{90}Ag_{10}$. The formation of a colourless solution indicates oxidative dissolution[29] of the NPs but this reactivity was not observed for the larger NPs, even on rapid addition of >100 mol% Au precursor. The different mechanism may be attributed to the larger surface area to volume ratio for the smaller NPs and the size dependent oxidation potential of Ag NPs. The standard redox potential of Ag decreases with decreasing diameter, increasing the potential difference in the oxidation of the Ag NPs and Au precursor.[30] In other words, oxidation will be more spontaneous for smaller diameter NPs. Rapid addition of Au^{3+} coupled with the 3:1 stoichiometric ratio for Au:Ag leads to dissolution of the Ag template before sufficient Au deposition occurs. As the reaction proceeds, the Au and Ag species are reduced by OAm forming Au-rich alloys.

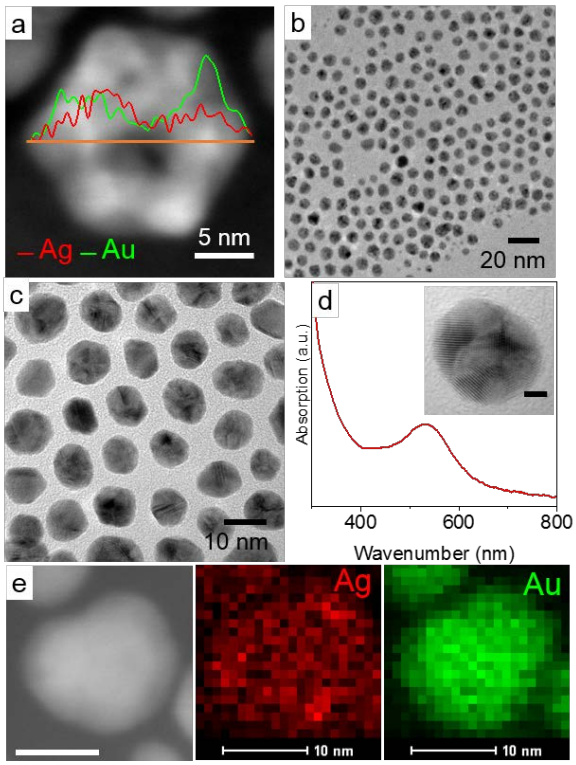

Conclusions

Galvanic replacement of Ag NP templates were studied in organic solvents. For single crystal NPs, formation of a Au shell around the template is facilitated the by the face centred cubic crystal structure and the almost identical lattice constants of Au (4.079Å) and Ag (4.086Å). Preferential deposition of Au onto {100} and {110} facets results in an octahedral morphology for both spherical (*i.e.* cuboctahedral) and cubic templates. The chemical composition of the NPs is size dependant with greater Au content obtained for smaller NPs, attributed to the faster diffusion in smaller NPs. For MTPs galvanic replacement can produce hollow and solid alloy NPs. Rapid precursor addition and higher reaction temperature favour the formation of solid alloy NPs. The lower stability of the polycrystalline alloys results in lower Au:Ag ratio compared to single crystal templates.

Acknowledgements

We thank Science Foundation Ireland Grant SFI/12/RC/2278 for supporting this research.

References

1. S. E. Skrabalak, J. Chen, Y. Sun, X. Lu, L. Au, C. M. Cobley and Y. Xia, *Acc. Chem. Res.*, 2008, **41**, 1587-1595.
2. H. A. Atwater and A. Polman, *Nat. Mater.*, 2010, **9**, 205-213.
3. G. Collins, M. Schmidt, C. O'Dwyer, J. D. Holmes and G. P. McGlacken, *Angew. Chem. Int. Ed.*, 2014, **53**, 4142-4145.
4. C. Shen, C. Hui, T. Yang, C. Xiao, J. Tian, L. Bao, S. Chen, H. Ding and H. Gao, *Chem. Mater.*, 2008, **20**, 6939-6944.
5. J. N. Anker, W. P. Hall, O. Lyandres, N. C. Shah, J. Zhao and R. P. Van Duyne, *Nat. Mater.*, 2008, **7**, 442-453.
6. P. K. Jain, X. Huang, I. H. El-Sayed and M. A. El-Sayad, *Plasmonics*, 2007, **2**, 107-118.
7. E. Gonzalez, J. Arbiol and V. F. Puntes, *Science*, 2011, **334**, 1377-1380.
8. X. Xia, Y. Wang, A. Ruditskiy and Y. Xia, *Advanced Materials*, 2013, **25**, 6313-6333.
9. A. K. Singh and Q. Xu, *ChemCatChem*, 2013, **5**, 652-676.
10. T. Shibata, B. A. Bunker, Z. Y. Zhang, D. Meisel, C. F. Vardeman and J. D. Gezelter, *J. Am. Chem. Soc.*, 2002, **124**, 11989-11996.
11. Y. D. Yin, R. M. Rioux, C. K. Erdonmez, S. Hughes, G. A. Somorjai and A. P. Alivisatos, *Science*, 2004, **304**, 711-714.
12. Y. G. Sun, B. T. Mayers and Y. N. Xia, *Nano Lett.*, 2002, **2**, 481-485.
13. Y. G. Sun and Y. N. Xia, *J. Am. Chem. Soc.*, 2004, **126**, 3892-3901.
14. Y. Sun, *Chem. Soc. Rev.*, 2013, **42**, 2497-2511.
15. X. Lu, H.-Y. Tuan, J. Chen, Z.-Y. Li, B. A. Korgel and Y. Xia, *J. Am. Chem. Soc.*, 2007, **129**, 1733-1742.
16. P. R. Selvakannan and M. Sastry, *Chem. Comm.*, 2005, DOI: 10.1039/b418566h, 1684-1686.
17. J. Yang, J. Y. Lee and H. P. Too, *J. Phys. Chem. B*, 2005, **109**, 19208-19212.
18. Y. Yin, C. Erdonmez, S. Aloni and A. P. Alivisatos, *J. Am. Chem. Soc.*, 2006, **128**, 12671-12673.
19. Karvianto and G. M. Chow, *J. Nanopart. Res.*, 2012, **14**.
20. X. Hong, D. Wang, S. Cai, H. Rong and Y. Li, *J. Am. Chem. Soc.*, 2012, **134**, 18165-18168.
21. L. Polavarapu and L. M. Liz-Marzan, *Nanoscale*, 2013, **5**, 4355-4361.
22. Y. Ma, W. Li, J. Zeng, M. McKiernan, Z. Xie and Y. Xia, *J. Mater. Chem.*, 2010, **20**, 3586-3589.
23. S. Peng, J. M. McMahon, G. C. Schatz, S. K. Gray and Y. Sun, *Proc. Natl. Acad. Sci. USA*, 2010, **107**, 14530-14534.
24. B. Goris, L. Polavarapu, S. Bals, G. Van Tendeloo and L. M. Liz-Marzan, *Nano Lett.*, 2014, **14**, 3220-3226.
25. M. McEachran, D. Keogh, B. Pietrobon, N. Cathcart, I. Gourevich, N. Coombs and V. Kitaev, *J. Am. Chem. Soc.*, 2011, **133**, 8066-8069.
26. Y.-H. Chien, M.-F. Tsai, V. Shanmugam, K. Sardar, C.-L. Huang and C.-S. Yeh, *Nanoscale*, 2013, **5**, 3863-3871.
27. W. H. Qi and S. T. Lee, *J. Phys. Chem. C*, 2010, **114**, 9580-9587.
28. S. Liu, G. Chen, P. N. Prasad and M. T. Swihart, *Chem. Mater.*, 2011, **23**, 4098-4101.
29. T. Pal, T. K. Sau and N. R. Jana, *Langmuir*, 1997, **13**, 1481-1485.
30. O. S. Ivanova and F. P. Zamborini, *J. Am. Chem. Soc.*, 2010, **132**, 70-72.